

Fault Monitoring Techniques for Nuclear Components

Gee-Yong Park¹ and Jung Taek Kim²

^{1,2}*Korea Atomic Energy Research Institute, Yuseong-gu, Daejeon, Dukjin-dong 150, South Korea*

*gypark@kaeri.re.kr
jtkim@kaeri.re.kr*

ABSTRACT

In this paper, we describe our previous studies for the development of an analysis algorithm and the application of a fault monitoring technique. Various signal processing methods have been implemented in the so-called monitoring tools to monitor and analyze abnormal conditions of components in nuclear power plants (NPPs). One of the analysis methods were devised by us for the efficient analysis of transient signals from NPP process components. This method, the adaptive cone-kernel distribution, is presented in this paper along with the description of the monitoring tool. Then, some application results using the monitoring tool are presented. As another application, the fault monitoring technique applied to the agitator driving system of a thermal chemical reduction reactor is also presented though this technique is not integrated in the monitoring tool yet.

1. INTRODUCTION

The fault monitoring technique consists of hardware and software elements to investigate successfully the status of a target component, equipment, or system. For the hardware part, a sensing type and an appropriate sensor for measuring relevant signals are first determined. Along with the sensors employed, the data acquisition system should be established. For the software part, it is usual in our studies that a signal processing method is selected to analyze the signal that were acquired by and stored in the data acquisition system, then some useful feature representing information of the target system status is extracted from the result of signal processing analysis, and finally a certain diagnostic method such as expert system or neural network is applied to the features, resulting in the identification of current status of the system to be monitored.

We implemented various signal analysis methods and improved some methods for application to the transient signals from a system. These various signal analysis

methods covers from classical analysis methods such as the frequency or spectral analysis to the time-frequency analysis methods for analysis of transient signals such metal impact signal by a loose part in NPP.

Figure 1 shows the main page of our monitoring tool. This tool has classical spectral analysis methods and also various time-frequency analyses such as STFT (Short-Time Fourier Transform), WVD (Wigner-Vill Distribution), CWD(Choi-Williams Distribution), BJD (Born-Jordan Distribution), CKD (Cone-Kernel Distribution), and ACKD (Adaptive Cone-Kernel Distribution). The monitoring tool was implemented by LabVIEW program language. The analysis methods described above were implemented into “dll” libraries that were then integrated into the LabVIEW-based monitoring tool

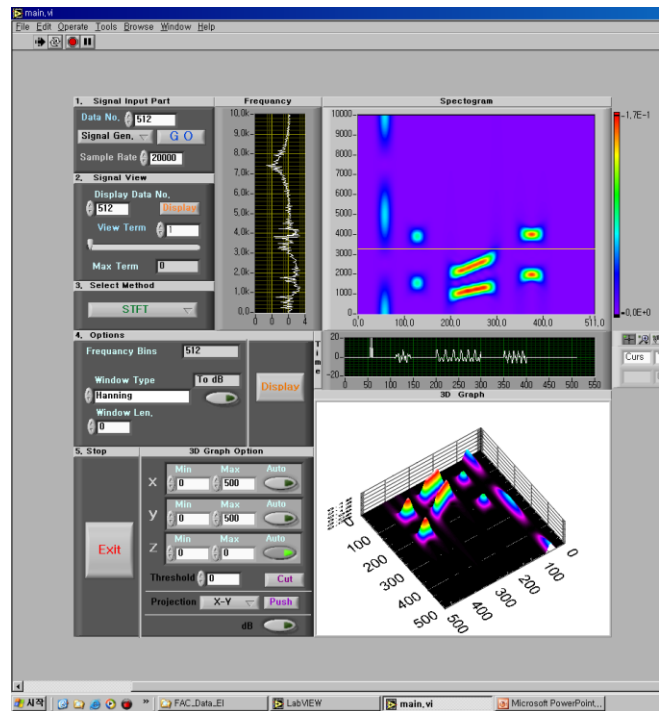


Figure 1. Monitoring tool - main page

The upper left part of Figure 1 indicates menus for reading input data and displaying this data and the lower left part is for menus for options and refining analysis results. The upper right screen is for displaying 2-dimensional time-frequency results along with frequency and time data. The lower graph is displayed only when 3 dimensional data need to be displayed. The more explanation of each component can be seen in Figure 2.

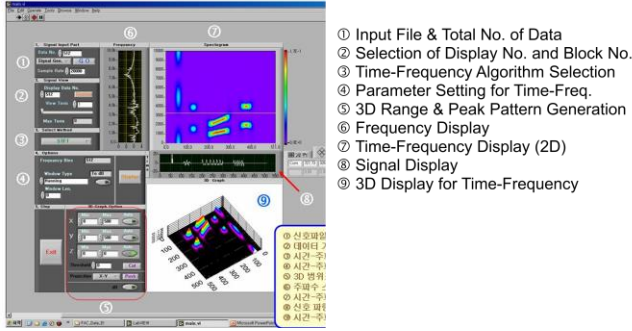


Figure 2. Menu functions of the monitoring tool

Among them, the adaptive cone-kernel distribution (ACKD) was devised by our team and this is described in detail in Section 2 with brief description of applications results. Section 3 describes other application result of fault monitoring techniques that had been carried out in our projects but are not implemented in this monitoring tool.

2. DEVELOPMENT OF ADAPTIVE CONE KERNEL DISTRIBUTION

In this section, an adaptive CKD, which was devised for improving analysis performance and also reducing calculation load, is described.

The general form of a time-frequency distribution (TFD) is represented by (Claasen & Mecklebrauker, 1980)

$$C_x(t, \omega; \phi) = \int_{-\infty}^{\infty} \int_{-\infty}^{\infty} \int_{-\infty}^{\infty} e^{j(\xi t - \tau \omega - \xi u)} \phi(\xi, \tau) x(u + \frac{\tau}{2}) x^*(u - \frac{\tau}{2}) du d\tau d\xi, (1)$$

where x is an analytic signal, x^* is the complex conjugate of x , τ represents the time lag, and ϕ is the kernel function. The form of TFD by Cohen (Cohen, 1995) is slightly different from Eq.(1) in that the parameter ξ has a negative sign. If the kernel function is such that $\phi(\xi, \tau) = 1$, then Eq.(1) is the Wigner-Vill distribution (WVD). The WVD is known to have very desirable properties in the time-frequency domain. For a signal composed of multi-component signals, however, it has a critical drawback in that ghost signals (i.e., called “cross-terms”) present among the true signal components. These results make the time-frequency representation very difficult to interpret. To overcome this, time-frequency representation of a signal is usually performed base on the general form of Eq.(1) where the kernel function ϕ is designed from the previously proposed candidates

(Hlawatsch & Boudreaux-Bartels, 1992) for a better representation of a case sensitive signal.

Various kernels have been proposed for satisfying the desirable properties (time and frequency maginals, finite support in time and frequency, and so forth) of TFD and at the same time reducing the undesirable effect (i.e., cross-terms). The exponential kernel, which is known as the Choi-Williams kernel (Choi & Williams, 1989), is the one that satisfies almost all of the desirable TFD properties and can suppress well the effects of the cross-terms. It is represented by

$$\phi(\xi, \tau) = e^{-\xi^2 \tau^2 / \sigma} (2)$$

In Eq.(2) σ is a tuning parameter. Born-Jordan kernel has the form of

$$\phi(\xi, \tau) = \sin c(\alpha \xi \tau) (3)$$

It fulfills almost all of the TFD properties. All the kernel functions are summarized well in the paper of Cohen (1995) and Hlawatsch and Boudreaux-Bartels (1992).

2.1. CKD and ACKD

Up to this time, there is no kernel that satisfies all the desirable properties and also shows the best cross-term reduction capability. The cone-kernel distribution proposed by Y. Zhao, et al (1990) is the one with the best capability of suppressing the cross-term effects; instead, of sacrificing many of desirable properties (Loughlin et al., 1993). The design of CKD is originated from the idea that a kernel should satisfy the time support and also enhancing the frequency resolution by paying a penalty to the neighbors of signal frequencies by the use of a so-called lateral inhibition (Zhao, et al., 1990). A different form of the general class of TFD of Eq.(1) can be presented such as

$$C_x(t, f; \phi) = \int_{-\infty}^{\infty} \int_{-\infty}^{\infty} \phi(t - u, \tau) x(u + \frac{\tau}{2}) x^*(u - \frac{\tau}{2}) e^{-j2\pi f \tau} du d\tau (4)$$

The kernel function in Eq.(4) is the inverse Fourier transform of the kernel function in Eq.(1) with respect to ξ . The cone kernel in the t - τ domain in (4) is represented as

$$\phi(t, \tau) = \begin{cases} g(\tau), & |\tau| \geq a |t| \\ 0, & \text{O.W.} \end{cases} (5)$$

In Eq.(5), the cone boundary parameter, a , adjusts the slopes of the cone with the constraint that $2 \leq a < \infty$ and usually set to 2 according to the finite support property (Claasen & Mecklebrauker, 1980). The function $g(\tau)$ is a sort of window in the Fourier transform for preventing a frequency leakage and it is usually represented by the Gaussian function.

The discrete form of the above equation (Czerwinski & Jones, 1995) is represented by

$$C_x(n, f; \text{CKD}) = \sum_{k=-T}^T g(k) \sum_{p=-|k|}^{|k|} x(n+p+k)x^*(n+p-k)e^{-j2\pi fk} \quad (6)$$

In Eq.(6), the continuous variable f will be represented by the discrete Fourier data at the implementation phase. According to the cone length T in Eq.(6), the resolutions of time and frequency domains are traded off.

For a signal with multi-components, it is necessary for the cone length to vary adaptively according to the signal type. The adaptive cone-kernel distribution (ACKD) was proposed by Czerwinski & Jones (1995) where the performance measure was the highest time-frequency signal energy normalized by the square of the cone length. This method usually shows a reasonably optimal value of the cone length according to the signal type, but it requires massive computations and a careful selection of the time-axis range for the signal data.

In this paper, a more computationally efficient adaptive method is proposed. In this method, at a particular time step n , the frequency values are calculated for each incremental step of a variation of the cone length. The performance measure is the normalized Shannon's entropy that is applied to the frequency data obtained at each incremental step in the cone length for a particular time. The normalized Shannon's entropy is expressed as

$$E(T, n) = \sum_{m=0}^{M-1} f_N(m, n, T) \ln \frac{1}{f_N(m, n, T)} \quad (7)$$

In Eq.(7), n is the time index and m is the discrete frequency index, M is the total frequency data. The f_N is the normalized energy and represented by

$$f_N(m, n, T) = \frac{|C_x(n, m; \text{CKD for } T)|^2}{\sum_{m=0}^{M-1} |C_x(n, m; \text{CKD for } T)|^2} \quad (8)$$

The optimal cone length T at a particular (fixed) time index is determined when the entropy has a local minimum value over the variations of the cone length T . If it is decreasing smoothly then the optimal T is determined when the entropy value is below the threshold value such as

$$E_{th} = E_{min} + \lambda(E_{max} - E_{min}) \quad (9)$$

In Eq.(9), E_{th} is the threshold entropy, E_{min} and E_{max} represent the minimum and maximum values of the entropy, respectively, and λ is the given threshold parameter. In determining the optimal cone length, the entropy trend shows a small fluctuating behavior, which may induce an inaccurate determination of the local minimum point. In order to remedy this problem, the entropy plot for the variation of T at a particular sample point is smoothed by the curve smoothing technique (Moon, 1998).

2.2. Performance Evaluation for Arbitrarily Synthesized Signal

Figure 3 shows an arbitrary, multi-component signal that contains two impulses at the data sample index $i=56$ and 60 , respectively, one burst signal at $i=108\sim 148$, two chirp signals at $i=200\sim 300$, and two mixed sine waves at $i=350\sim 400$. The sampling rate is given by 50 kHz. The detailed information of the multi-components (S1, S2, S3, S4, and S5) is presented in Table 1.

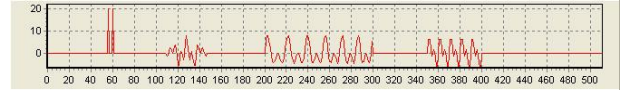


Figure 3: An arbitrarily generated signal

Table 1. Description of signal components

Signals	Expression & Description
#1 (S1)	$S1 = 20$ at $i=56$, and $S1 = 0$, otherwise
#2 (S2)	$S2 = 20$ at $i=60$, and $S2 = 0$, otherwise
#3 (S3)	$S3 = 4M\{\cos(2\pi \times 20 \times i/256) + \cos(2\pi \times 50 \times i/256)\}$, and $M = \begin{cases} 1 - \frac{1}{400}(i-128)^2 & ,108 \leq i \leq 148 \\ 0 & , \text{Otherwise} \end{cases}$
#4 (S4)	$S4 = 4\{\cos(2\pi \times (i/8) \times (i/512)) + \cos(2\pi \times (i/16) \times (i/512))\}$, for $200 \leq i \leq 300$, and $S4=0$, otherwise
#5 (S5)	$S5 = 4\{\cos(2\pi \times i/5) + \cos(2\pi \times i/10)\}$, for $200 \leq i \leq 300$, and $S5 = 0$, otherwise

Figure 4 displays the results of the STFT, the Born-Jordan distribution (BJD), the Choi-Williams distribution (CWD), the Cone-Kernel distribution (CKD) and the adaptive CKD (ACKD). Figure 4(a) represents the STFT with the window length of 64, which shows clearly the superior depression of the cross-terms but very poor time and frequency resolutions. The BJD in Figure 4(b) is obtained from the parameter $\alpha = 0.005$ in Eq.(3). The CWD with $\sigma=150000$ in Eq.(2) is displayed in Figure 4(c), where the cross-terms are still disturbing the time-frequency representation. Figure 4(d) displays the CKD with $T=32$ in Eq.(6). All the figures depict the real part. Though the CKD with an appropriate cone length ($T=32$) shows a better the time-frequency representation than the other time-frequency representations in Figures 4(a),(b), and (c), it is necessary the cone length be varied according to the signal type.

Figure 4(e) shows the result of the ACKD proposed in this paper. The maximum search range of the cone length is given by 64 and the threshold parameter is set by $\lambda = 0.05$. Figure 4(e) shows a good time-frequency representation and moreover, the two vertical strips for corresponding impulse signals can be discriminated. Figure 5(a) and Figure 5(b) magnify the results of ACKD of Figure 4(e) and CKD of

Figure 4(d), respectively, for the data sample range of 0~100. As can be seen in Figures 5, the discrimination of the two impulses are much clearer in ACKD. The optimal values of the cone length calculated in this adaptive method are shown in Figure 6 along the data sample index.

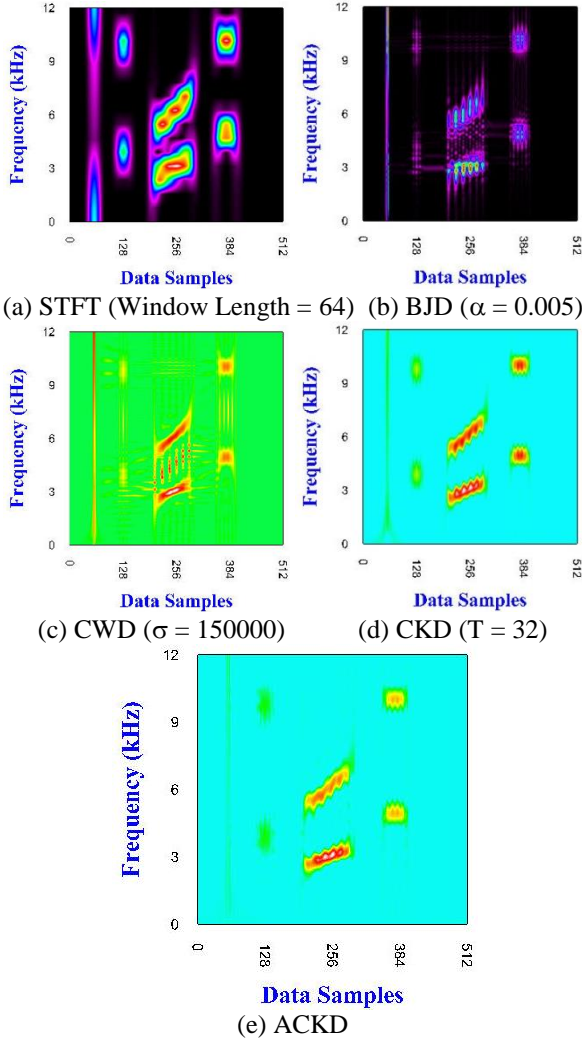


Figure 4: Time-Frequency representations for an arbitrarily generated signal

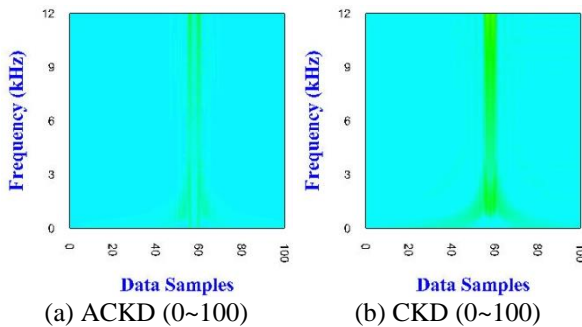


Figure 5: Comparison of magnified ACKD and CKD



Figure 6: Optimal cone length along signal sequence

2.3. Application of Monitoring Tool

The monitoring tool as in Figure 1 was used for monitoring of the integration of a check valve and also for identifying the status of pipe corrosion, which had been performed by the joint research between the KAERI and the SNL (Sandia National Laboratory) as an I-NERI project.

Some example of application of ACKD to acoustic emission (AE) sensor signals for the check valve monitoring is depicted in Figure 7.

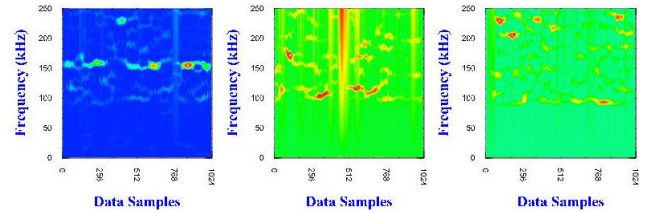


Figure 7: Results of ACKD for AE signals from a check valve disk

As can be seen in Figure 7, the AE signals from a healthy check valve typically have a signal component dominant at 150 kHz and, if an abnormal situation happens, there can be seen that signal components dominant at other frequencies begin to appear. When the leak occurs due to disk wearing, the dominant frequencies are extensively spreading over 100 kHz as can be seen in Figure 7(b). For the disk stuck by a foreign object, it can be seen that the signal components at higher frequencies are generated.

For the identification of pipe corrosion, it was identified that the signals from accelerometers installed in the area of the pipe elbow did not represent distinguishable transient characteristics in such a passive method (in other words, in the case of two transmitting- and receiving- accelerometers, a certain discriminating feature was supposed to be identified.) For the experiment for the pipe corrosion, the STFT was applied to signals from accelerometers and the linear scale of the distribution of STFT was transformed into the log scale. The ridge pattern is extracted from this result. Figure 8 shows the ridge pattern for the pipe in the normal state.

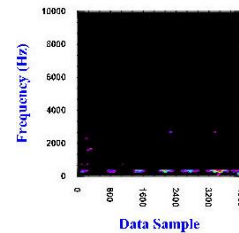
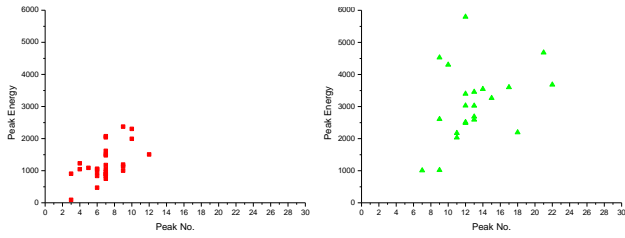


Figure 8: Ridge pattern for the pipe with normal state

The ridge pattern in Figure 8 was abstracted by the use of peak number and peak energy. Figure 9 shows some application results from the two types of experimental pipes; the pipe with normal state and 2 mm mechanical thinning.



(a) Normal state (b) 2 mm thinning

Figure 9: Peak number vs. peak energy for pipes with different local width

As can be seen in Figure 9, the abstracted ridge pattern is moving from the lower left portion to the upper right portion. This shift trend could be identified consistently for the pipe with 1 mm thinning, and was validated for the real data from the pipe corrosion.

3. APPLICATION OF FAULT MONITORING TECHNIQUE

This section presents additional application example from our previous study (Park et al., 2003) that are not integrated into the monitoring tool in Section 2. The target system to which a fault monitoring technique was applied is the agitator driving system. The agitator driving system equipped on the top of the thermal reduction reactor for a high-temperature chemical reaction is composed of the magnetic driver and the agitator whose rotating axis is connected to the motor installed on the side of the thermal reduction reactor via the flexible joint.

Figure 10 shows the configuration of the thermal reduction reactor and the agitator driving system. The power transmission through the flexible joint produces vibrations and, for series of the operations, this induces the looseness of the surrounding bolts. In the real operations, there existed that the operator sometimes forgot to tighten some of bolts.

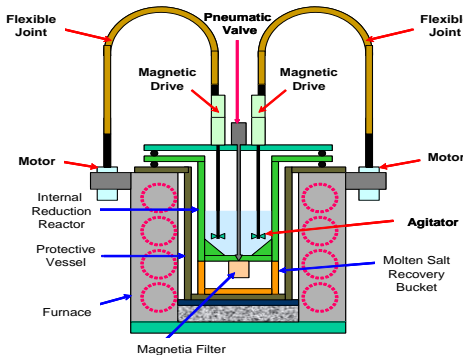


Figure 10. Configuration of the full-scale thermal reduction reactor and the agitator driving system

During the thermal reduction process, the fume is generated from the chemical reaction and propagates through the internal space of the agitator driving system. The bearings in the magnetic driver are affected by the fume, which results in the corrosion/wear of the bearings and the blocking of the clearance between the rotating axis and the outer ring.

The fault in the agitator driving system increases the burden of regulating the agitator rotating speed to the pre-set point (200 rpm) for the optimal chemical reaction. In order to identify the fault occurrence and its cause, the fault monitoring technique for the agitator driving system is developed. This technique is implemented on the vibration signals measured by two accelerometers on the outer shroud of the magnetic drive as shown in Figure 11.

Through the experiments, the vibration signals for a speed of 200 rpm with various faults were measured. The sampling rate was set to 25.6 kHz for all cases. The data for 5 types of faults are analyzed. The five faults presented in this paper are the clearance blocking, the bearing defects, the lower bolts looseness, the upper bolts looseness, and the upper-right bolt looseness.

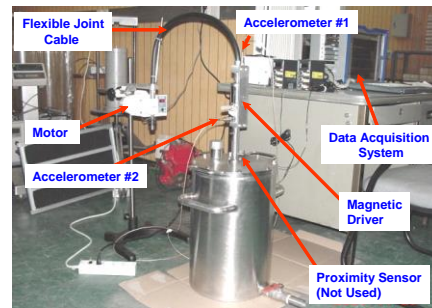


Figure 11. Experimental facility for the agitator driving system

The rotation speed is fluctuated with the maximum deviation of ± 20 rpm around 200 rpm. In order to classify the faults, the spectral analysis was first applied to the signals for 5 faults and the normal rotation. From the spectral analysis, some faults such as the clearance blocking and the bearing defects show slightly different trend other than the normal rotation but it is not easy to identify the distinguishing peaks for discriminating a fault.

In order to identify accurately a fault in the agitator driving system, the wavelet decomposition (Burrus, et al., 1998) was applied to the vibration signal. Figure 12 shows the wavelet decomposition for a normal vibration signal that has 65,536 data samples. As can be seen in Figure 12, the vibration signals are decomposed into the corresponding components that have the octave band frequency contents. The feature extraction was performed by the 2nd order moment calculation. The 2nd order moment calculation was simple and showed good distinguishable features for corresponding faults as can be seen in Figure 13. For

establishing the diagnosis process, the neural network classifier, which is called Fuzzy ARTMAP (Carpenter, et al., 1992), was constructed.

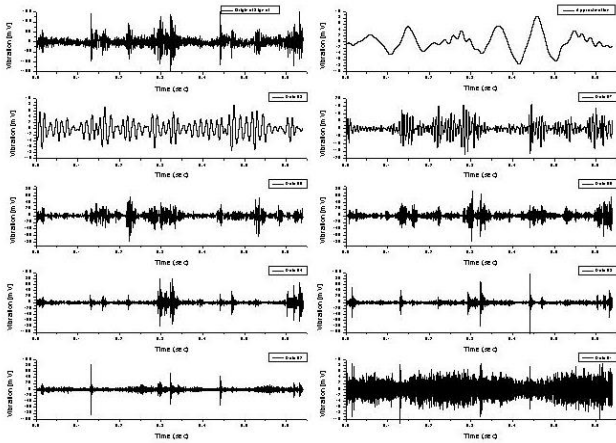


Figure 12. Wavelet decomposition for normal signal

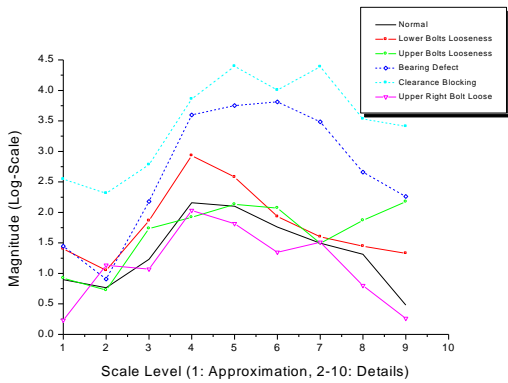


Figure 13. Features extracted from the results of wavelet decomposition for 6 types of cases

The fuzzy ARTMAP is a class of neural networks that perform incremental supervised learning of recognition categories and multidimensional maps in response to input vectors presented in arbitrary order. Figure 14 shows the architecture of the fuzzy ARTMAP where two fuzzy ART (Carpenter, et al., 1991) modules (ART_a and ART_b) and a map field F_{ab} are involved. The input vectors **A** of dimension M_a and **B** of dimension M_b are the feature vectors respectively corresponding to the symptom and the cause. The components of each input vector are analog or binary values within the range of [0,1]. The each component of the input vector represents a feature item that is grouped to establish the representative feature. Thus the analog value of each component of the input vector means the degree of belongingness to the corresponding feature item, and this is similar to the fuzzy membership value. The detailed

description on the operational mechanisms of the fuzzy ARTMAP is presented in Carpenter, et al (1992).

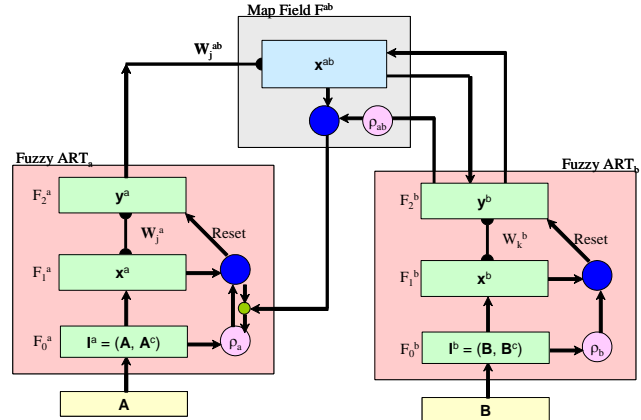


Figure 14. Configuration of fuzzy ARTMAP

During training the fuzzy ARTMAP, one set for each fault was selected from the data set and the remainder data set were used to test the fuzzy ARTMAP performance. In the training phase, training data for each fault is presented just once to the fuzzy ARTMAP and single learning iteration is performed. The input vector **A** for the fuzzy ART_a is the 2nd momentum feature values and has a dimension of M_a = 9. All the inputs for the fuzzy ART_a are normalized. The input vector **B** for the fuzzy ART_b is the binary values with a single '1' that represent a specific fault and has a dimension of M_b = 6. Figure 15 summarizes the test data and the parameters for the fuzzy ARTMAP. From tests, the fuzzy ARTMAP showed the perfect fault identification though some test data are distorted from the training data.

Training Data	• Data Set : 6 Cases (1:Normal, 2:Upper-Right Bolt Loose, 3: Lower Bolts Loose, 4:Upper Bolts Loose, 5:Bearing Defect, 6:Clearance Blocking)
Test Data	• Normal Data : 7 Sets • Upper-Right Bolt Looseness : 4 Sets • Lower Bolts Looseness: 5 Sets • Upper Bolts Looseness: 3 Sets • Bearing Defects: 4 Sets • Shaft Clearance Blocking: 4 Sets
Training Type & Parameters	• Off-Line Learning, Single Input Presentation, and Single Learning Iteration • Fast Learn: $\beta=1$ • Conservative Limit Value: $\alpha=0.0001$ • Vigilance and Matching Criterion: $\rho_a = 0.8, \rho_b = 0.8, \rho_{ab} = 0.8$
Test Results	• For Training Data : 100 % Correct Identification • For Test Data: 100 % Correct Identification

Figure 15. Parameter settings of the fuzzy ARTMAP and the diagnosis results for faults

4. CONCLUSIONS

In this paper, the monitoring tool established at our department and the fault monitoring techniques using this tool and other means are briefly described. In the nuclear field, classical analysis methods such as a spectral analysis or an auto-regressive model are applicable to most of signals

stored in the data acquisition system. For a more delicate analysis for transient signals, an analysis method based on the time-frequency basis is useful. In this paper, an adaptive cone-kernel distribution whose window size is varied according to its adaptive mechanism is presented. This method is so efficient for computing time that it can be used on line. The monitoring tool described in this paper contains various signal-analysis methods. In our works, this tool was applied to the monitoring of the check valve and the identifying the status of pipe corrosion. By the use of the monitoring tool we developed, a new method or technique can be easily implemented and incorporated into this tool.

As one additional application, the fault monitoring technique of the agitator driving system was described. In this monitoring technique, the wavelet decomposition is used as a signal processing analysis and 2nd order momentum is used to extract the signal features from the decomposed signals. For investigating or diagnosing the fault status, the fuzzy ARTMAP is employed for discriminating robustly the fault patterns. These signal processing algorithm and fault monitoring technique are also going to be implemented in the monitoring tool.

REFERENCES

- Burrus, C. S., Gopinath, R. A., & Guo, H. (1998), *Introduction to Wavelets and Wavelet Transforms*, Prentice Hall.
- Claasen, T. A. C. M., & Mecklebrauer, W. F. G. (1980), The Wigner Distribution – A Tool for Time-Frequency Signal Analysis; Part III-Relations with Other Time-Frequency Signal Transforms. *Philips J. of Research*, vol.35, no.6, pp.372~389.
- Cohen, L. (1995), *Time-Frequency Analysis*, Prentice-Hall.
- Choi, H. I., & Williams, W. J. (1989), Improved Time-Frequency Representation of Multicomponent Signals using Exponential Kernels. *IEEE Transactions on Acoustics, Speech, and Signal Processing*, vo.37, no.6, pp.862~871.
- Czerwinski, R. N., & Jones, D. L. (1995), Adaptive Cone-Kernel Time-Frequency Analysis. *IEEE Transactions on Signal Processing*, vol.43, no.7, pp.1715~1719.
- Hlawatsch, F., & Boudreaux-Bartels, G. F. (1992), Linear and Quadratic Time-Frequency Signal Representations. *IEEE SP Magazine*, pp.21~67, April.
- Loughlin, P. J., Pitton, J. W., & Atlas, L. E. (1993), Bilinear Time-Frequency Representations: New Insights and Properties. *IEEE Transactions on Signal Processing*, vol.41, no.2, pp.750~767.
- Moon, B. S. (1998), A Curve Smoothing Method by Using Fuzzy Sets. *Fuzzy Sets and Systems*, vol.96, pp.353~358.
- Park, G. Y., et al. (2003), Fault Diagnosis for Agitator Driving System in a High Temperature Thermal Reactor. *Nuclear Engineering and Technology*, vol.35, no.5, pp.454~470.
- Zhao, Y., Atlas, L. E., & Marks II, R. J. (1990), The Use of Cone-Shaped Kernels for Generalized Time-Frequency Representations of Nonstationary Signals. *IEEE Transactions on Acoustics, Speech, and Signal Processing*, vol.38, no.7, pp.1084~1091.

BIOGRAPHIES

Gee-Yong Park Dr. Gee Yong Park achieved Ph.D. degree at the Department of Nuclear Engineering in Korea Advanced Institute of Science and Technology (KAIST) in 1996. Since then, he has been involved in Department of I&C and Human Factors of Korea Atomic Energy Research Institute (KAERI). His major research area includes the controller design and the monitoring and diagnosis of nuclear power plants, software reliability, and cyber security.

Jung Taek Kim Mr. Jung Taek Kim is in course of Ph.D. degree at the Department of Electronic Engineering in Chungnam National University (CNU) since 2002. He is working in Division of I&C and Human Factors of Korea Atomic Energy Research Institute (KAERI) during 26 years. His major research area includes a design of the alarm processing system and the monitoring and diagnosis system of nuclear power plants.